# Propagation Characteristics of Elastic Wave in High-speed railway Embankment and Its Application to Defect Detection

M. Chen[1], S. K. Feng[1], A. L. Che[1], H. Wang[1]

[1]School of Naval Architecture, Ocean and Civil Engineering, Shanghai Jiaotong University, Shanghai 200240; feng.sjtu@sjtu.edu.cn

**ABSTRACT:** The defects in high-speed railway embankment will grow during operation. It will bring potential risk to railway safety. In order to develop an efficient detection method for the defects in embankment, a numerical simulation and field model test are carried out to study the influence of defect on wave propagation in embankment. A three-dimensional model to embankment and finite element method is employed, and the characteristics of wave form, amplitude response, and particle motion of sampling point on the slab are taken into account. The field entity model is a full scale one, and it is built with materials in accord with the real railway embankment, and their construction methods are all the same. Elastic wave is excited by impacting on the surface of the entity model slab using a rubber hammer, the wave field is observed by vertical geophones on the slab. Common offset gather and common source gather are recorded for seismic imaging and elastic wave analysis. The result of simulation agrees well with that of field test qualitatively. It shows that the seismic imaging technique is effective for detecting embankment defects immediate under the slab.

## 1 INTRODUCTION

Modern means of railway transportation in China are being currently developed at a rapid pace. The velocity of high-speed railway is nowadays over 300 km/h. At the same time, the “high-speed” requires high quality of embankment, various defects such as differential settlement, cracks in the slab, local loose zone in the embankment and so on may lead to a sever safety risk. Although there is a progress in the analysis of the causes of these problems (Kaynia et al. 2000; Hall 2003; Vostroukhov et al. 2003; Ling et al. 1999), the detection methods to reveal internal defects could not adapt to high accuracy requirement at concrete slabs of embankment. The rebound method which measures the rebound distance after its impact on the surface of media can only give the surface strength of concrete structure with low precision (Kim et al. 2009). The ground penetration radar (GPR), which is often used at present, cannot provide a result related to the concrete strength. In addition, The GPR is also easily influenced by the condition of test media like containing steel reinforcements (Shaw et al. 2005). The ultrasonic method cannot be

applied to the underground geotechnical investigation due to fast attenuation (Akkaya et al. 2003). These factors lead to the pursuit of better nondestructive testing methods used in geotechnical engineering.

Meanwhile the propagation of elastic wave in half-space layered media has created growing concern, which gradually provides a deeper insight into the subject. Similar to the seismic reflection method in petroleum exploration, impacting on the surface of geotechnical media generates surface wave, S-wave and P-wave (Vai et al. 1999). The media structure could be probed from the intensity of reflection wave as well as dispersion characteristics of Rayleigh wave. Although normally the vertical component of the wave field works well for imaging simple layered media (Paulsson et al. 2004), the application of this method is not common in civil engineering, especially in high-speed railway embankment (HRE).

Two-dimensional (2D) simulation for wave propagation in layered media has previously been used to analyze inhomogeneous media vertically (Liu et al. 2013). The 2D cross section results were described, which is not enough to reveal complex media. Three-dimensional (3D) simulation can more accurately display the characteristics of the elastic wave field. In this paper, the relationship among amplitude of wave, S-wave velocity and density is discussed by theoretically. A 3D model for embankment and finite element method is employed. Furthermore field test is a full scale model that has been built with the materials and construction in accord with the real railway. The results from the finite element analyses are compared with actual measurements as average amplitude response profiles could be utilized to be a basis for detection.

## 2 ELASTIC WAVES IN LAYERED MODEL

As shown in Fig. 1, when elastic wave travels through elastic and density interface with different properties, it will be partially reflected back and partially transmitted into the medium on the other side of the interface. The wave field should satisfy the boundary conditions in each interface, and can be regarded as both reflection and refraction waves. This media response is rather complicated due to consist of P-wave, S-wave and surface waves as well as converted waves.

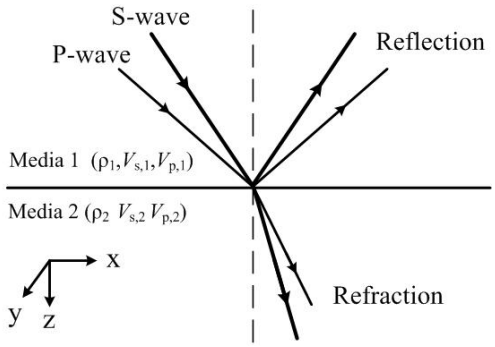


**FIG. 1. Wave propagation on an interface**

When P-wave incident onto the interface vertically, there is only reflection of P-wave in media 1. In that case, it makes easier to calculate the reflection coefficient without considering the influence of converted wave. Assuming that $A_1$ denotes the amplitude of incident P-wave in media 1; $A_2$ denotes the amplitude of reflected P-wave in media 1. The reflection coefficient $R_p$ can be expressed as,

$$R_p = \frac{A_2}{A_1} = \frac{\rho_2 V_{p,2} - \rho_1 V_{p,1}}{\rho_2 V_{p,2} + \rho_1 V_{p,1}} \quad (1)$$

Similarly, only S-wave should be considered in the case that the S-wave incident onto the interface vertically. Thus the reflection coefficient $R_s$ can be expressed as,

$$R_s = \frac{A_2}{A_1} = \frac{\rho_2 V_{s,2} - \rho_1 V_{s,1}}{\rho_2 V_{s,2} + \rho_1 V_{s,1}} \quad (2)$$

Where $\rho_i$ ($i$=1,2) is the density of media $i$; $V_{s,i}$ and $V_{p,i}$ are the wave velocity of S-wave velocity and P-wave in media $i$ respectively; φ, ψ denote the scalar potential of P-wave and S-wave respectively.

From the Eq. 1 and Eq. 2, reflection coefficient is related to physical properties of the tests material. And it can also be determined from the amplitudes of the incident and the reflected wave. Fig. 2 shows the case that seismic wave generated by impact travels through the interface with different properties. If the offset of observation point from the source is short enough in respect to the thickness of the media 1, the amplitude of wave can be express as,

$A_1 = A_0R_1$

$A_2 = A_1R_0R_1 = A_0R_1^2R_0$, ……

$A_p = A_{p-1}R_0R_1 = A_0R_1^pR_0^{p-1}$, ……

$A_n = A_{n-1}R_0R_1 = A_0R_1^nR_0^{n-1}$

$A = A_0 + A_1 + A_2 + \ldots\ldots = \Sigma (A_j)$, j=1, 2, 3, ……

Where A is seismic wave received by the receiver; $R_0$, $R_1$ are the reflection coefficient of the free surface and interface respectively. The density of the air above media 1 is so small that the reflection coefficient $R_0$ is close to -1. It indicates that amplitude of wave change with physical properties of the tests material and can be defined as a basis for distinguishing between interfaces with different material.

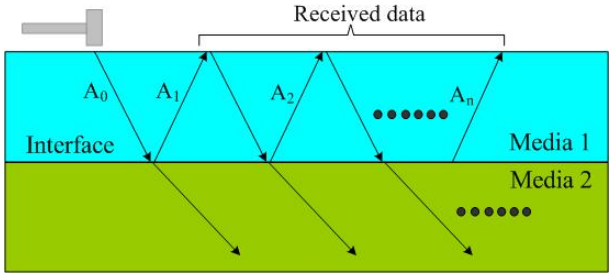


**FIG. 2. Concept of multiples**

## 3 NUMERICAL SIMULATION

### 3.1 Modeling

3D finite element model of HRE, performed to study the wave propagation, is transformed into a symmetry model. The 3D numerical railway embankment model is shown in Fig.3 (a), which consists of three parts, a concrete slab in the upper part of the model is about 0.54 m in depth, the following part is a concrete basement with a thickness of 0.3 m, and the other part is a defect at a depth of 54 cm below the embankment surface. The local loose area inside the model is set as 0.5×0.5×0.15 $m^3$ and filled by some other soft material. With the respect to the size of defect area, the model is divided by hexahedron elements whose minimum size is 0.1m in both width and height, as shown in Fig.3 (b). It consists of 125,168 elements and 141,948 nodes. The bottom boundary of embankment is connected to infinite regions in order to absorb P-wave and S-waves.

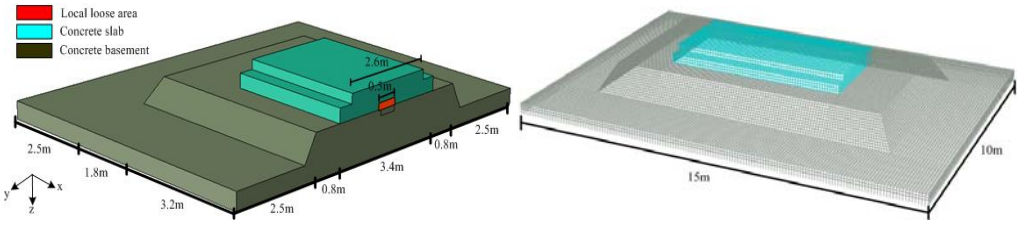


(a) Geometry and size (b) Finite element mesh

**FIG. 3. 3D numerical model**

The material parameters of the model are shown in table 1, where $\rho$ is the density of material, $E$ is the modulus, and $\mu$ denotes the Poisson's ratio. And the defect inside the model is considered as a local loose area. Fig. 4 shows the wave form of source. The excitation of elastic wave is conducted by continuous dynamic loads containing the time of 0.01024 seconds. And the measurement line is set in direction $y$.

**Table 1. Material parameters used in simulation**

| layer | $\rho$ kg/$m^3$ | E GPa | $M$ |
|---|---|---|---|
| Concrete slab | 2400 | 34.5 | 0.2 |
| Local loose area | 1100 | 0.001 | 0.45 |
| Concrete basement | 2300 | 25 | 0.25 |

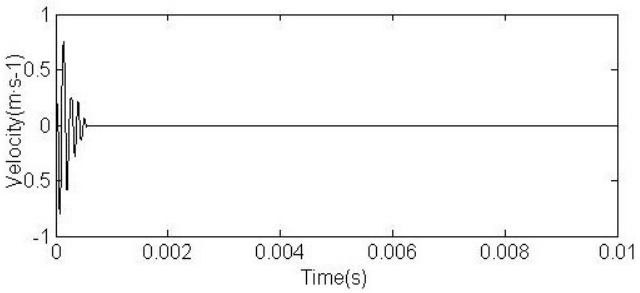

**FIG. 4. Wave form of the source**

### 3.2 Data analysis and results

For the thickness of slab is quite thin that the reflected waves arrive at the embankment surface before the available dynamic loads are applied to end, the response captured from embankment surface includes reflected signals as well as a lot of direct waves, which will greatly weaken the ratio of reflected waves. Moreover there exists strong refection on the sides of free boundary.

Fig. 5 shows the wave form of vertical velocity in *z* direction corresponding to distance 0.2 m from the input point. It can be observed that the amplitude response of wave form captured from the area over the defect is larger than that from the healthy area. It can be considered as caused by the reflection from the defect area. Compared with concrete slab, the material strength of the defect is much weak so that the reflected wave energy is almost close to that of incident wave. In order to clarify the wave propagation, the particle motion of sampling point on the slab is analyzed as shown in Fig. 6. The particle moves along with elliptic curve, which means Rayleigh wave is the dominant component part.

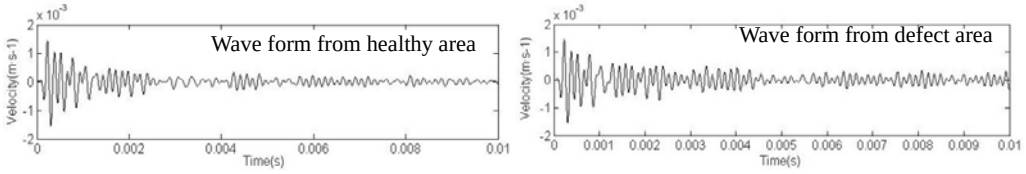


**FIG. 5. Wave form of vertical velocity**

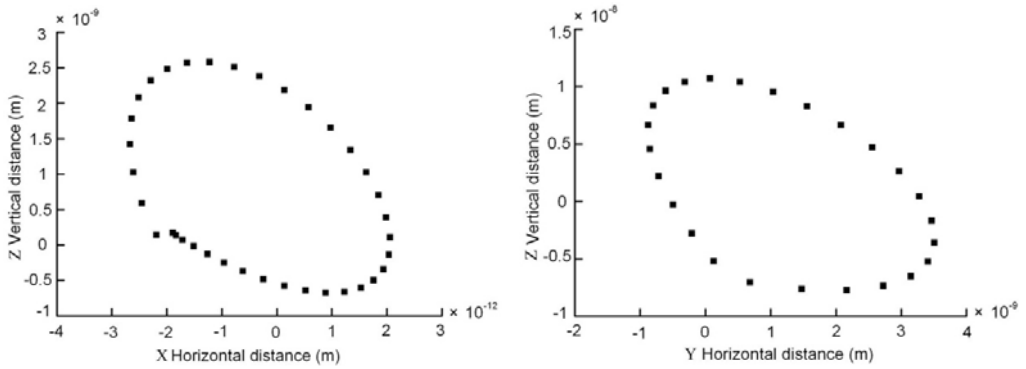


**FIG. 6. Particle motion at sampling point**

Fig. 7 shows the distribution of the amplitude response, which is normalized by the value at the healthy (None defect) area. Because the density and wave velocity of the defect is much smaller than those of the concrete, so the reflection coefficient is greater in defect area. And the value at the defect area should be greater than 1.0. Thus the amplitude response could be considered as an index to evaluate the region of defect quantitatively.

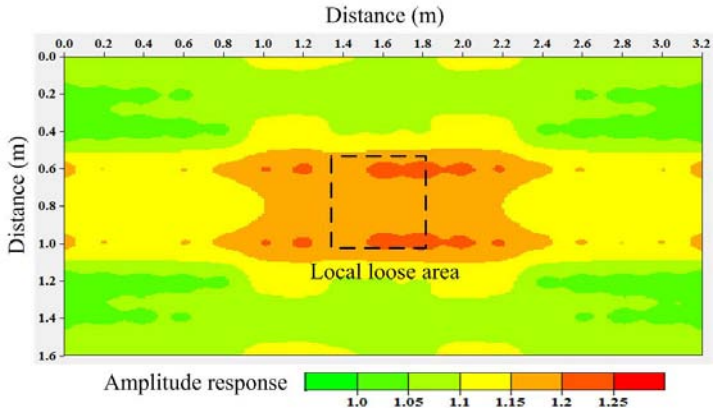


**FIG. 7. Distribution of amplitude response**

## 4 MODEL TESTS FOR DETECTING DEFECT

### 4.1 Overview of the tests

All the operations in this program, including experimental installation and acquisition, are carried out at the experimental site in Zhengzhou University. The model is built with the materials and construction in accord with the real railway. Its site condition, assembly parts and process of installation are presented in Fig. 8. It also describes the structure of railway embankment with three parts, track slab, support plate and basement. The track slab and support plate are made of steel reinforced concrete about 6.45 meters long. As one can see that a layer of clay is considered for good coupling of two slabs. At the bottom of embankment, there is a concrete basement with a thickness of 1.0 m, which could provide a solid base for train operation. The cavity with 0.5m×0.5m×0.15m$^3$ inside basement, which is located in the center of the bottom of the support plate, is the target to detect in this study.

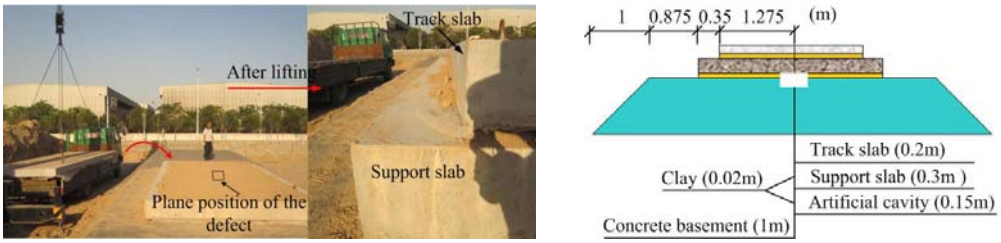


**FIG. 8. Experimental model and its structure**

### 4.2 Data acquisition and analysis

In the test procedure, a suit of seismic exploration instruments is used for capturing the ground response. Digital seismograph (Geode) with 24-channel (Ch) and 24-bit A/D conversion is used as the data acquisition system. Vertical velocity geophones with 4.5 Hz natural frequency together with a suit of coupling device are

used for receiving the ground response excited by a 0.454 kg rubber hammer. Fig. 9 shows the details of the layout of survey line on the slab. $L_i$ ($i$ = 1, 2, 3, …, 21) represents a survey line, and each line is arranged by a total of 12 survey points. The interval between two points is 0.2 m. The response of the ground is captured by the geophones in the distance 0.2 m from the impact face which is distributed at the side of geophones.

Fig. 10 shows the wave form of the survey line $L_{10}$ across the defect inside the base, the vertical axis is record time and transverse axis indicates the position of receiver. It is shown that there exists an evident increase of seismic amplitude in the distance ranging from 0.6 m to 1.2 m. Fig. 11 shows the amplitude response of the survey line. It is shown that the values of amplitude tend to rise and fall with the record position. The values of $L_{18}$ and $L_{21}$ make change but nearly remain a smooth level. However the maximal values of $L_{10}$ in local loose area is twice higher than that in dense area, as it is observed in previous simulation.

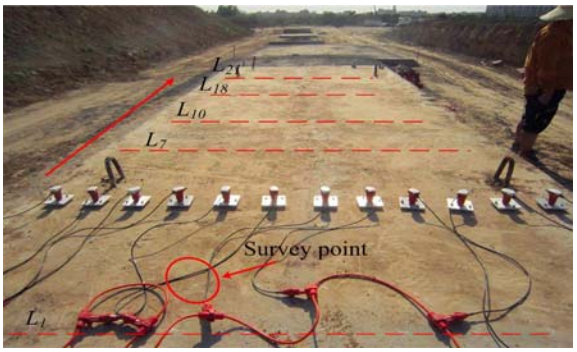


**FIG. 9. Distribution of survey line**

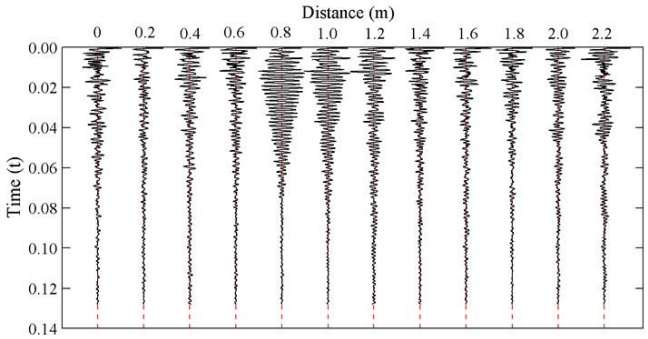


**FIG. 10. Wave form of $L_{10}$**

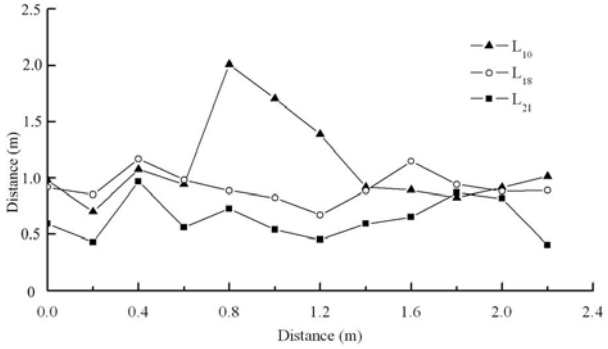


**FIG. 11. Amplitude of survey lines**

### 4.3 Evaluation of the region of defect

For different elastic properties between healthy and defect area, so there exists the difference in interface reflection. The phenomenon observed above two figures can be mostly attributed to the influence of multiple reflections at the defect surface. It suggests that interface reflection is sensitive to elastic properties of material on the wave propagation. Thus the region of defect in the layered media could be detected based on the comparison of amplitude.

Fig. 12 shows the amplitude response profiles in two dimensions measured by a total of 21 survey lines on the slab. There exists a gap between two slabs due to poor couple so that the wave will reflect back from interface. Although the model test is influenced by external factors, the region with red color at the center, located in the range of 1.6 m to 2.2 m, is evaluated as the local loose area coinciding with the reality well. Applying the amplitude as a basis for detection, the technique is achieved in the model test.

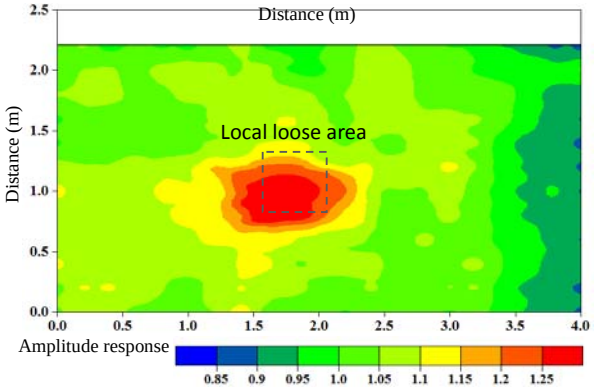


**FIG. 12. Distribution of amplitude response**

## 5 CONCLUSIONS

The relationship among amplitude of wave form, S-wave velocity and density is discussed theoretically. It concludes that amplitude of wave form change with physical properties of the tests material and can be defined as a basis for detection.

Wave form, amplitude response profiles and particle motion of sampling point from different area are compared by 3D finite element analyses. The amplitude response of the received wave form is considered as an index to evaluate the region of defect quantitatively. And it is also shown that Rayleigh wave is the dominating wave type.

Based on the result of simulation, model test is carried out for the defect in embankment and the result agrees with that of simulation qualitatively. The imaging method of elastic wave propagation provided an excellent nondestructive examination to detect local loose area.

## REFERENCES

Akkaya, Y., Voigt, T., Subramaniam, K. V. (2003). "Nondestructive measurement of concrete strength gain by an ultrasonic wave reflection method." *Materials and Structures*, 36(8):507-514.

Hall, L. (2003). "Simulations and analyses of train-induced ground vibrations in finite element models." *Soil Dynamics and Earthquake Engineering*, 23(5): 403-413.

Kaynia, A. M., Madshus, C., Zackrisson, P. (2000). "Ground vibration from high-speed trains: prediction and countermeasure." *Journal of Geotechnical and Geoenvironmental Engineering*, 126(6):531-537.

Kim, J. K., Kim, C. Y., Yi, S. T. (2009). "Effect of carbonation on the rebound number and compressive strength of concrete." *Cemment & Concrete Composites*, 31(2):139-144.

Ling, B., Cai, Y. (1999). "Dynamic analysis on subgrade of High-speed railways in geometric irregular condition." *Journal of the China Railway Society*, 21(2):84-88.

Liu, C., Che, A. L., Feng, S. K. (2013). "Propagation characteristics of elastic wave in layered medium and applications of impact imaging method." *J. Shanghai Jiaotong Univ.*, 18(3):1-7.

Paulsson, B., Karrenbach, M., Milligan, P. (2004). "High resolution 3D seismic imaging using 3C data from large downhole seismic arrays." *First Break*, 23:73-83.

Shaw, M. R., Millard, S. G., Molyneaux, T. C. K. (2005). "Location of steel reinforcement in concrete using ground penetrating radar and neural networks." *NDT & E International*, 38(3):203-212.

Vostroukhov, A. V., Metrikine, A. V. (2003). "Periodically supported beam on a visco-elastic layer as a model for dynamic analysis of a high-speed railway track." *International Journal of Solids and Structures*, 40(21):5723-5752.

Vai, R., Castillo-Covarrubias, J. M., Sánchez-Sesma, F. J. (1999). "Elastic wave propagation in an irregularly layered medium." *Soil Dynamics and Earthquake Engineering*, 18(1):11-18.